Journal of Sound and Vibration 329 (2010) 2450–2462

Contents lists available at ScienceDirect

Journal of Sound and Vibration

journal homepage: www.elsevier.com/locate/jsvi

Generalisation and optimisation of semi-active, on–off switching controllers for single degree-of-freedom systems

Jack N. Potter *, Simon A. Neild, David J. Wagg

Department of Mechanical Engineering, University of Bristol, Bristol BS8 1TR, UK

ARTICLE INFO

Article history:
Received 1 July 2009
Received in revised form
26 November 2009
Accepted 7 December 2009
Handling Editor: J. Lam
Available online 1 February 2010

ABSTRACT

This paper examines generalised forms of semi-active switching control in comparison to the sky-hook semi-active controller. A switching time controller is proposed and analysed, in order to determine the optimal performance, with regard to displacement transmissibility, of semi-active switching control. In addition, the model is also used to assess the optimality of the sky-hook switching conditions. An analytical solution is then derived for the optimal switching times. A generalised form of linear switching surface controller is then presented. It is demonstrated that this controller can produce near optimal performance.

1. Introduction

Semi-active dampers are a class of energy dissipating device for which the damping may be controlled in real-time. This is achieved by either altering the properties of the damping fluid, as is the case for electro- and magneto-rheological dampers [1], or by actuating mechanical components of the damper, an example of which is a variable orifice damper. Semi-active damping, as a method of vibration isolation, has been applied to many mechanical and civil engineering systems, see for example [2–7] and references therein. It has been demonstrated to provide considerably improved performance compared to vibration isolation through passive damping alone.

Approaches to the design of semi-active damping controllers can broadly be grouped into two forms. The first class applies to systems which may be accurately described using low order models, such as automotive suspension systems, for which simple pragmatic control approaches, based on reasoned physical argument, are often employed, for example [4,8–10,5,11].

As the complexity of a system increases it becomes difficult to generate semi-active control policies based on intuitive logic. Consequently for this second class of system, examples of which include cables, buildings and bridges, it is common for modified forms of active control design to be applied. A common example of this class of semi-active control is termed clipped-optimal control [12,9]. This employs conventional linear-quadratic regulator or linear-quadratic gaussian optimal control design based on linear system models, with the addition of saturation limits due to the physical constraints on the force that may be generated by the semi-active damper. This semi-active design approach has been applied to a number of civil engineering structures, for example see [13–18].

This paper is concerned with the first class of semi-active controller design. The most common form of control in this class is called sky-hook control, which is a control policy that can be applied when a semi-active damper is connected directly to a mass that is to be isolated. The sky-hook controller acts to increase damping when the damping force is acting

* Corresponding author.
E-mail addresses: jack.potter@bristol.ac.uk (J.N. Potter), simon.neild@bristol.ac.uk (S.A. Neild), david.wagg@bristol.ac.uk (D.J. Wagg).

0022-460X/$ - see front matter © 2009 Elsevier Ltd. All rights reserved.
doi:10.1016/j.jsv.2009.12.011

to dissipate energy from the mass. This paper seeks, through analysis of the sky-hook controller, to generalise this class of semi-active control in order to improve performance and better understand the mechanics that determine the optimality of the control design.

Firstly a review of a sky-hook control law and its behaviour when applied to a single degree of freedom, base excited suspension system is presented. A generalised form of switching control based on predetermined switching times is then proposed. Through simulation of this controller, the optimal performance, with regard to minimising displacement transmissibility, of this class of semi-active control is determined. The sky-hook controller is compared to these results in order to assess the optimality of the sky-hook switching conditions. An analytical solution for the optimal switching times, based on a harmonic balance of switching controlled system, is then presented. It is then shown how the sky-hook controller may be considered to be a specific case of a generalised form of state-dependent, linear switching surface controller. Through simulation, optimal switching surfaces are plotted and compared to the sky-hook surfaces. It is demonstrated numerically that, over a range of frequencies, the optimal switching surfaces may be approximated using the linear switching surface controller. The optimal switching surface control described in this paper is of appropriate form to apply to any system where conventional sky-hook control is applied. Examples of potential applications include automotive suspension systems [10] and seat suspensions [2].

The main technical novelty of this paper concerns the consideration of the common sky-hook semi-active controller [8] as a specific case of a more generalised form and the identification of the optimal case of this general form (in terms of optimal switching times and surfaces).

2. Sky-hook control

This paper will consider the semi-active isolation of a single degree-of-freedom base excited system such as that shown in Fig. 1(a), where m is the mass to be isolated, k is the suspension stiffness, c is a semi-active damper, x is the mass displacement and r is the base displacement. The system is harmonically excited at frequency, Ω, and displacement amplitude, Δ, such that $r=\Delta\sin\Omega t$. Using the standard normalised parameters; natural frequency, $\omega_n=\sqrt{k/m}$, and damping ratio, $\zeta=c/(2\sqrt{km})$, the equation of motion of the system may be written as follows:

$$\ddot{x}+2\zeta\omega_n(\dot{x}-\dot{r})+\omega_n^2(x-r)=0. \tag{1}$$

A common strategy for semi-active isolation of a such a system, proposed by Karnopp et al. [8] is to control the damper so that it emulates the behaviour of an idealised sky-hook system. Such a system, as shown in Fig. 1(b), features an inertially grounded passive damper, c_{sky}, connected to the mass to be isolated, providing a damping force that is always resistant to the mass's velocity. A commonly used semi-active approximation of the sky-hook system, often referred to as on–off sky-hook control, is to set the damping to a high level when the damping force is dissipative with regard to the kinetic energy of the mass and to set the damping to a low level otherwise. For the system shown in Fig. 1(a), this corresponds to increased damping when the damper velocity and absolute mass velocity are of the same sign. An on–off sky-hook control law for this system may be expressed as follows, where ζ_h and ζ_l denote high and low damping ratios, respectively,

$$\zeta=\begin{cases}\zeta_h, & \dot{x}(\dot{x}-\dot{r})>0,\\ \zeta_l, & \text{else.}\end{cases} \tag{2}$$

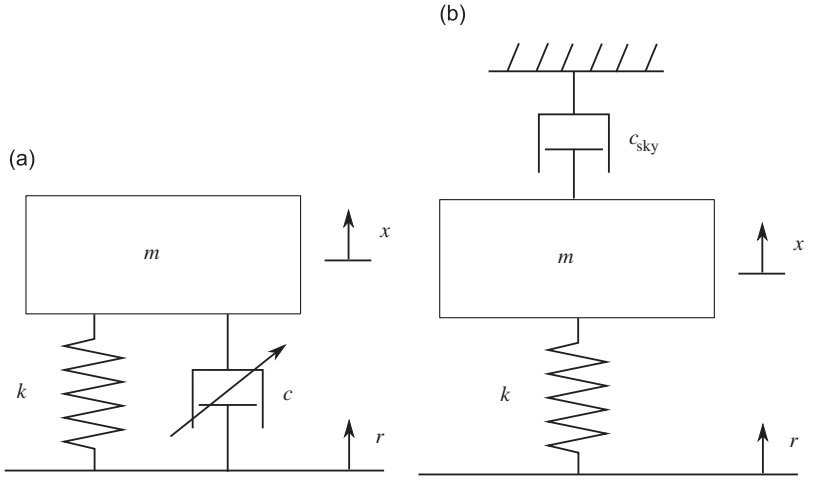

Fig. 1. Mechanical models of (a) semi-active base excited suspension system and (b) idealised sky-hook system.

The sky-hook form of control law can be susceptible to chatter [4]. This occurs when, upon switching from high to low damping at $\dot{x}=0$, the spring force is of opposite sign and of greater magnitude than the low damping force. Under this condition, the net force on the mass will change direction upon switching to the low damping state, pushing the velocity back toward zero and consequently the low to high switching. This results in rapid switching between the high and low damping levels until the system states are such that the low damping force is of greater magnitude than the spring force. This phenomenon is typically associated with large differences between the high and low damping values. This study will be limited to values of damping for which chattering does not occur.

A typical plot of displacement transmissibility is shown in Fig. 2, from which it can be seen that the sky-hook controller performs better than passive damping at lower frequency but at higher frequency produces higher transmissibility than the low level passive damping. From this it can be inferred that the sky-hook controller must be a sub-optimal form of on–off semi-active control as it fails locate the lower amplitude solution provided by the always off state.

As is clear from Eq. (2), the sky-hook controller switches damping levels at the zero crossings of the mass and damper velocities. These switching conditions can be considered as two switching surfaces of $\dot{x}=0$ and $\dot{x}-\dot{r}=0$ and can be illustrated in a plane of system velocities as shown in Fig. 3. The shaded region of this figure corresponds to that in which the damping force is dissipative with regard to the kinetic energy of the mass and is the region within which the sky-hook control law increases damping.

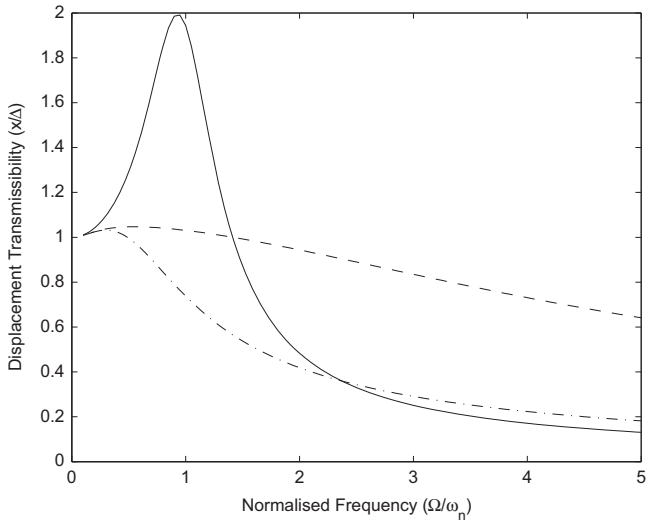

Fig. 2. Transmissibility of passively damped and sky-hook systems for $\zeta_h=2$ and $\zeta_l=0.3$: — passive damping $\zeta=\zeta_l$, − − − passive damping $\zeta=\zeta_h$, − · − · − on–off sky-hook control.

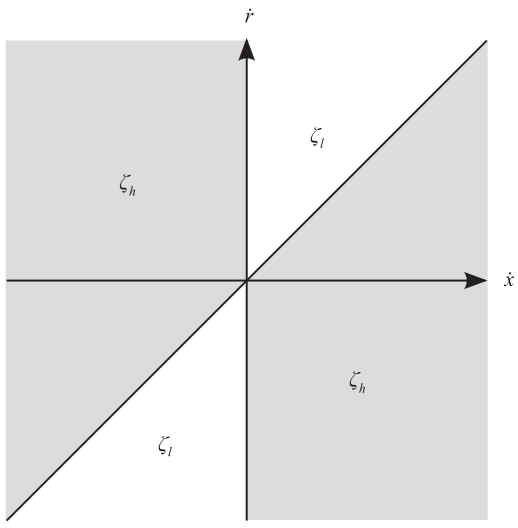

Fig. 3. Illustration semi-active switching surfaces of sky-hook controller.

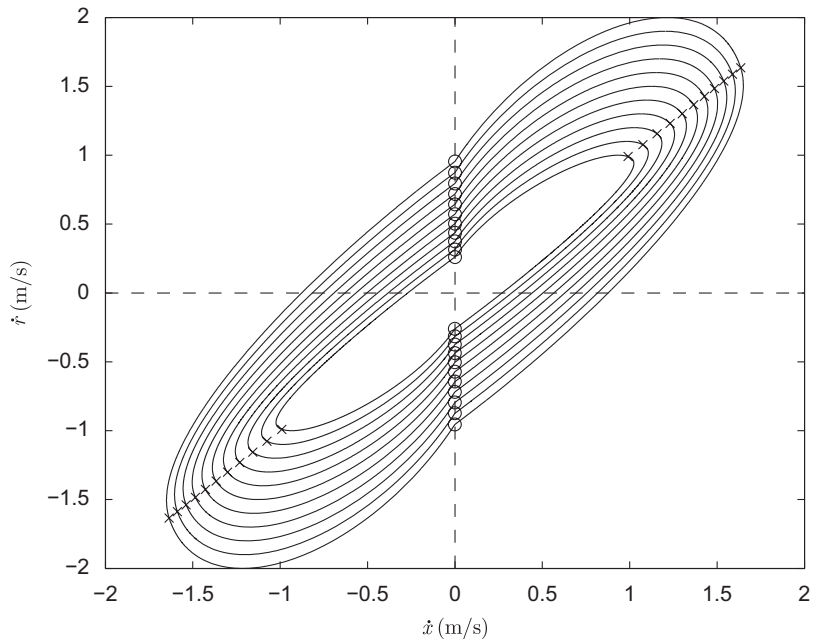

Fig. 4. Steady state velocities and switching states of the sky-hook controller over the frequency range $\Omega/\omega_n = 1-4$ for $\zeta_h = 2$, $\zeta_l = 1$: ○ high to low switching, × low to high switching.

The function of these switching surfaces can be seen by plotting the steady-state system velocities within this plane, an example of which is shown in Fig. 4, in which the high to low switching states are denoted by circles and the low to high switching states denoted by crosses. At each frequency the velocity trajectory forms a closed orbit, these orbits move outwards from the centre with increasing frequency. It can be seen that in the steady-state, the velocity trajectory crosses each of the switching surfaces once every half period of excitation. Consequently, at a given frequency, the damping level is switched from high to low and back at fixed times every half period.

By generalising the controller switching conditions, in terms of switching times and switching surfaces, this study seeks to identify an optimal form of semi-active switching controller and understand the mechanics which cause the optimal solution to differ from the sky-hook control scheme.

3. Switching time control

In this section we will examine the response of a generalised form of semi-active switching control, with arbitrarily defined switching times. The controller we propose is illustrated in Fig. 5, where the high to low switching time is denoted by t_1 and the low to high switching time by t_2. Analysis of this generalised controller form, for all permissible switching times, will allow the optimal response of this class of switching controller to be determined. This may then be compared with the response of the sky-hook controller, in which t_1 and t_2 are governed by the conditions given in Eq. (2), in order to assess the optimality of the sky-hook switching conditions.

3.1. Numerical analysis

Parameters are introduced for frequency normalised width, $\bar{t}$, and centre of the damping peak, t_0. These are illustrated in Fig. 5 and relate to the switching times as follows:

$$t_1 = \begin{cases} (t_0 - \bar{t}/2 + \pi)/\Omega, & t_0 - \bar{t}/2 < 0, \\ (t_0 - \bar{t}/2)/\Omega, & \text{else} \end{cases} \tag{3}$$

and

$$t_2 = \begin{cases} (t_0 + \bar{t}/2 - \pi)/\Omega, & t_0 + \bar{t}/2 > \pi, \\ (t_0 + \bar{t}/2)/\Omega, & \text{else.} \end{cases} \tag{4}$$

The parameters, t_0 and $\bar{t}$, can have values between the limits of zero and π, and together can describe the system for all permissible switching times. The motivation for introducing these parameters is to aid subsequent analysis and allow results to be presented in a clearer form.

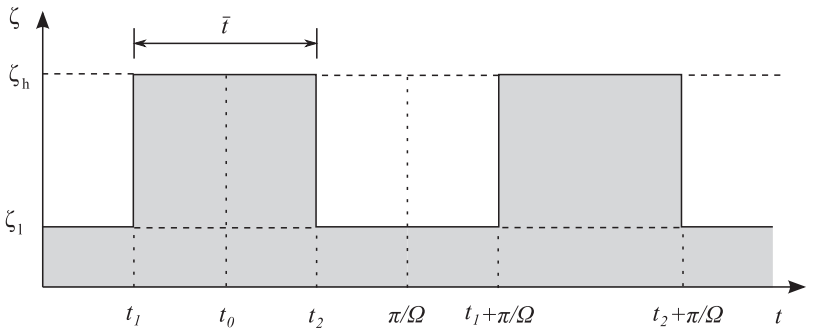

Fig. 5. Illustration of switching times over an excitation period.

Simulations are computed for a range of t_0 and $\bar{t}$ values between the minimum and maximum values. Typical results are shown in Fig. 6. The upper edge, $\bar{t}=\pi$, corresponds to the passive high damping response and the lower edge, $\bar{t}=0$, corresponds to the passive low damping response. The minimum steady-state displacement response is denoted by a diamond and the sky-hook steady-state response is denoted by a circle. Note that presenting these contour plots for $\bar{t}$ and t_0 produces a continuous surface. If the results were presented in terms of t_1 and t_2, the surface would be discontinuous along $t_1=t_2$, corresponding to the switch from high to low passive damping either side of the line.

These results show a single, clear minima, revealing the existence of distinct, optimal switching times at each frequency. A general trend, present regardless of damping values, is the movement of the minima from high to low $\bar{t}$ values with increasing frequency. This shows that to minimise transmissibility, the high damping level should be applied for smaller proportions of the excitation period as frequency increases. An analogy may be drawn between this result and optimisation of an equivalent passively damped system, which requires lower levels of damping with increasing frequency to minimise transmissibility.

Below, and close to, the undamped natural frequency, the sky-hook switching conditions produce switching times very close to optimal. However, as frequency increases, the sky-hook switching times can be seen to diverge from the optimal. Most notably, the sky-hook controller results in larger $\bar{t}$ values than are optimal. This shows that essentially the sky-hook switching conditions apply more damping than is necessary, to the detriment of control performance.

As the numerical results reveal the sky-hook controller to be sub-optimal, we now seek an analytical solution for the optimal switching times.

3.2. Analytical optimisation

Frequency analysis of the system at optimal switching times, an example of which is shown in Fig. 7, reveals that the response is dominated by the excitation frequency. This suggests that a harmonic balance (for example see [19]) at the excitation frequency is a suitable method for the analytical solution of the switching time controlled system. This technique is now applied to the system.

Defining, $z=x-r$, Eq. (1) may be rewritten as

$$\ddot{z}+2\zeta(t)\omega_n\dot{z}+\omega_n^2 z=-\ddot{r}. \tag{5}$$

Considering the displacement response only at the excitation frequency, z may be expressed as follows:

$$z\approx a_1\cos\Omega t+b_1\sin\Omega t. \tag{6}$$

By substituting Eq. (6) into Eq. (5), multiplying by $\sin\Omega t$ and integrating across an excitation period, the following expression is obtained, noting the orthogonality condition that when integrated the $\sin\Omega t\cos\Omega t$ terms are eliminated:

$$\pi(\omega_n^2-\Omega^2)b_1+2\omega_n\Omega^2 b_1\int_0^{2\pi/\Omega}\zeta(t)\cos\Omega t\sin\Omega t\,\mathrm{d}t-2\omega_n\Omega^2 a_1\int_0^{2\pi/\Omega}\zeta(t)\sin^2\Omega t\,\mathrm{d}t=\Delta\pi\Omega^2. \tag{7}$$

For $t_2>t_1$, the damping applied by the switching time controller may be expressed as follows, where τ is the modulo of time, t, and a half excitation period, π/Ω

$$\zeta=\begin{cases}\zeta_h, & t_1<\tau<t_2,\\ \zeta_l, & \text{else}.\end{cases} \tag{8}$$

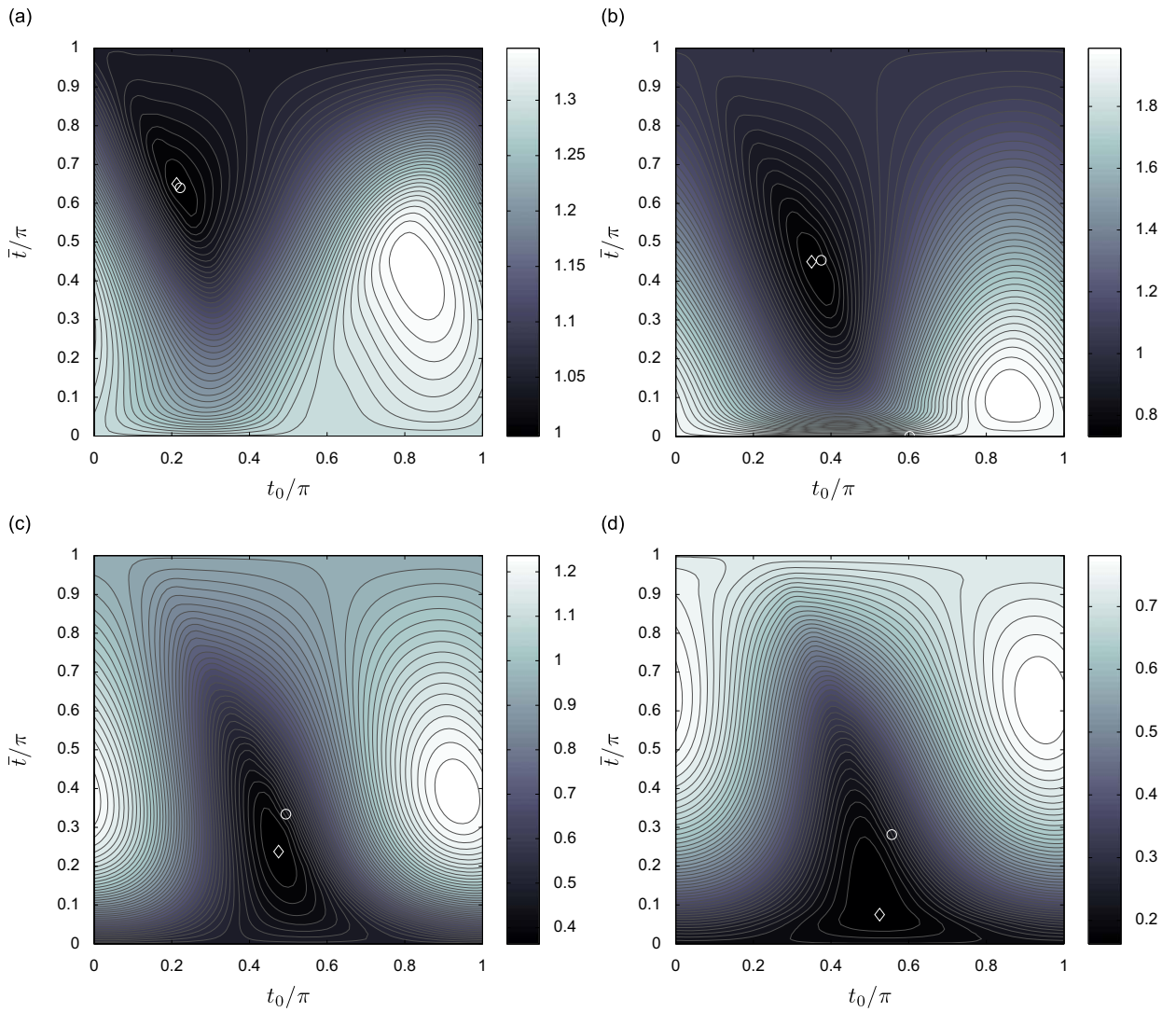

Fig. 6. Displacement transmissibility contour plots of switching time controller for $\zeta_h = 2$, $\zeta_l = 0.3$ and $\Omega/\omega_n =$ (a) 0.5 (b) 1 (c) 2 (d) 4: ◇ optimal switching times, ○ sky-hook switching times.

By substituting the switching controller from Eq. (8) into Eq. (7) and evaluating the integrals we obtain

$$2\omega_n\left(\Omega\frac{\zeta_h-\zeta_l}{\pi}(t_2-t_1)+\zeta_l+\frac{\zeta_h-\zeta_l}{2\pi}(\sin 2\Omega t_1-\sin 2\Omega t_2)\right)a_1 + \left(-(\omega_n^2-\Omega^2)/\Omega-2\omega_n\left(\frac{\zeta_h-\zeta_l}{\pi}(\sin^2\Omega t_2-\sin^2\Omega t_1)\right)\right)b_1 = -\Delta\Omega. \tag{9}$$

Similarly, substituting Eqs. (6) and (8) into Eq. (5), multiplying by $\cos\Omega t$ and integrating across an excitation period, produces the following:

$$\left((\omega_n^2-\Omega^2)/\Omega-2\omega_n\frac{\zeta_h-\zeta_l}{\pi}(\sin^2\Omega t_2-\sin^2\Omega t_1)\right)a_1 + 2\omega_n\left(\Omega\frac{\zeta_h-\zeta_l}{\pi}(t_2-t_1)+\zeta_l+\frac{\zeta_h-\zeta_l}{2\pi}(\sin 2\Omega t_2-\sin 2\Omega t_1)\right)b_1 = 0. \tag{10}$$

Using Eqs. (3) and (4), Eqs. (9) and (10) may be rewritten as functions of $\bar{t}$ and t_0, giving

$$2\omega_n\left(\zeta_l+\frac{\zeta_h-\zeta_l}{\pi}(\bar{t}-\sin\bar{t}\cos 2t_0)\right)a_1-\left((\omega_n^2-\Omega^2)/\Omega+2\omega_n\frac{\zeta_h-\zeta_l}{\pi}\sin\bar{t}\sin 2t_0\right)b_1 = -\Delta\Omega \tag{11}$$

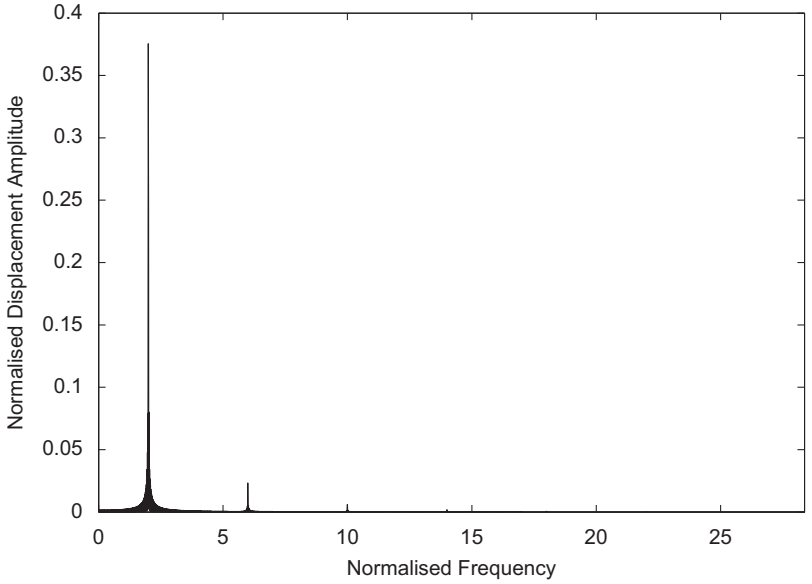

Fig. 7. Steady state frequency content of x for $\zeta_h = 3$, $\zeta_l = 0.2$ and $\Omega/\omega_n = 2$. Axes are normalised relative to excitation frequency and amplitude.

and

$$\left((\omega_n^2 - \Omega^2)/\Omega - 2\omega_n \frac{\zeta_h - \zeta_l}{\pi} \sin\bar{t} \sin 2t_0\right) a_1 + 2\omega_n \left(\zeta_l + \frac{\zeta_h - \zeta_l}{\pi}(\bar{t} + \sin\bar{t}\cos 2t_0)\right) b_1 = 0. \tag{12}$$

By solving Eqs. (11) and (12), the following expressions for a_1 and b_1 are obtained:

$$a_1 = \frac{-2\Delta\omega_n\Omega^3\left(\zeta_l + \frac{\zeta_h - \zeta_l}{\pi}(\bar{t} + \sin\bar{t}\cos 2t_0)\right)}{4\omega_n^2\Omega^2\left(\left(\frac{\zeta_h - \zeta_l}{\pi}\bar{t} + \zeta_l\right)^2 - \left(\frac{\zeta_h - \zeta_l}{\pi}\right)^2 \sin^2\bar{t}\right) + (\omega_n^2 - \Omega^2)^2} \tag{13}$$

and

$$b_1 = \frac{\Delta\Omega^2\left(\omega_n^2 - \Omega^2 - 2\omega_n\Omega\frac{\zeta_h - \zeta_l}{\pi}\sin\bar{t}\sin 2t_0\right)}{4\omega_n^2\Omega^2\left(\left(\frac{\zeta_h - \zeta_l}{\pi}\bar{t} + \zeta_l\right)^2 - \left(\frac{\zeta_h - \zeta_l}{\pi}\right)^2 \sin^2\bar{t}\right) + (\omega_n^2 - \Omega^2)^2}. \tag{14}$$

The steady state displacement amplitude of x, $\bar{x}$, may be written as follows:

$$\bar{x} = (a_1^2 + (b_1 + \Delta)^2)^{1/2}. \tag{15}$$

Substituting Eqs. (13) and (14) into Eq. (15) produces the following approximate solution for the steady-state displacement response of the switching time controlled system

$$\bar{x}^2 = \left(\frac{-2\Delta\omega_n\Omega^3\left(\zeta_l + \frac{\zeta_h - \zeta_l}{\pi}(\bar{t} + \sin\bar{t}\cos 2t_0)\right)}{4\omega_n^2\Omega^2\left(\left(\frac{\zeta_h - \zeta_l}{\pi}\bar{t} + \zeta_l\right)^2 - \left(\frac{\zeta_h - \zeta_l}{\pi}\right)^2 \sin^2\bar{t}\right) + (\omega_n^2 - \Omega^2)^2}\right)^2 + \left(\frac{\Delta\Omega^2\left(\omega_n^2 - \Omega^2 - 2\omega_n\Omega\frac{\zeta_h - \zeta_l}{\pi}\sin\bar{t}\sin 2t_0\right)}{4\omega_n^2\Omega^2\left(\left(\frac{\zeta_h - \zeta_l}{\pi}\bar{t} + \zeta_l\right)^2 - \left(\frac{\zeta_h - \zeta_l}{\pi}\right)^2 \sin^2\bar{t}\right) + (\omega_n^2 - \Omega^2)^2} + \Delta\right)^2. \tag{16}$$

A similar derivation may be performed for $t_1 > t_2$, however, due to the definitions of the switching times in Eqs. (3) and (4), the solution reached is the same as that found for the $t_2 > t_1$ case.

When compared to the numerical solution of the switching controlled system, this analytical approximation is seen to be accurate at higher frequency, but is less accurate close to and below the undamped natural frequency of the system.

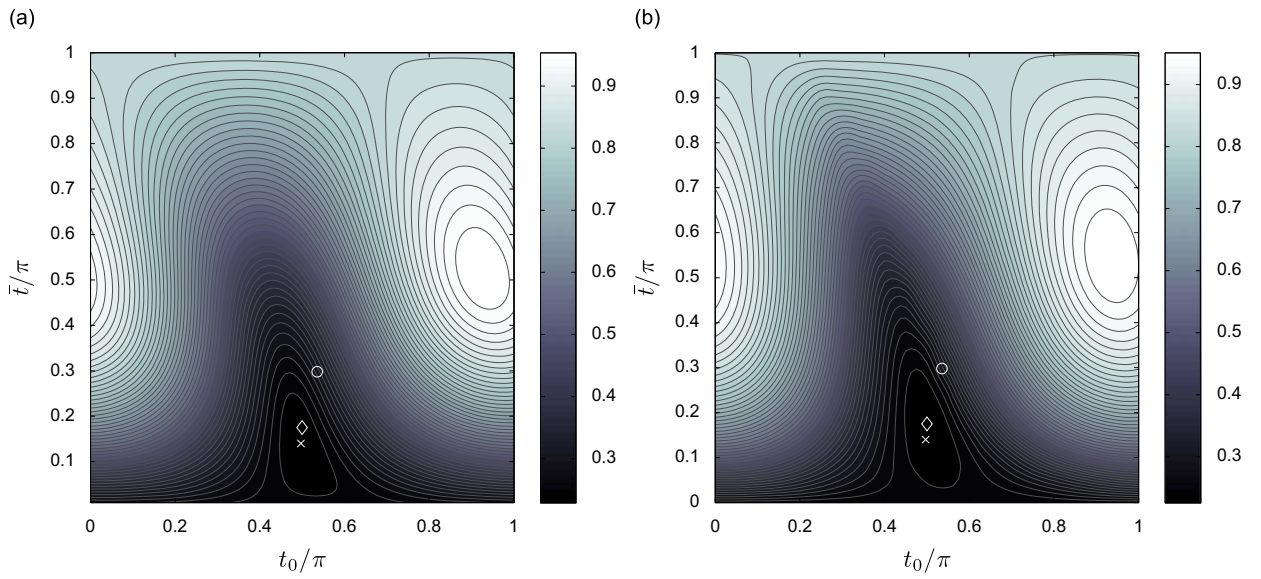

Fig. 8. Transmissibility contour plots for $\Omega/\omega_n = 3$, $\zeta_h = 2$ and $\zeta_l = 0.3$. (a) Analytical approximation using Eq. (16). (b) Numerical solution: ◇ optimal switching times, ○ sky-hook switching times, × analytical optimal switching times.

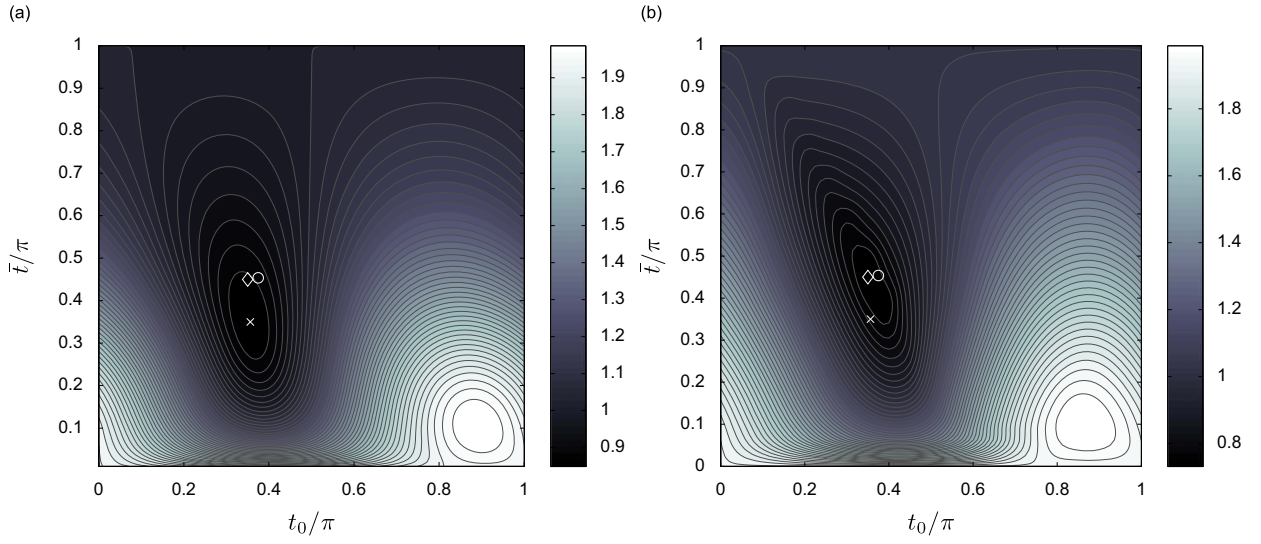

Fig. 9. Transmissibility contour plots for $\Omega/\omega_n = 1$, $\zeta_h = 2$ and $\zeta_l = 0.3$. (a) Analytical approximation using Eq. (16). (b) Numerical solution: ◇ optimal switching times, ○ sky-hook switching times, × analytical optimal switching times.

Typical results are shown in Figs. 8 and 9, in which the numerical minima is denoted by a diamond, the analytically approximated minima denoted by a cross and the sky-hook solution by a circle. At low frequency the analytical minima is further from the actual minima than the sky-hook solution. At higher frequencies, where the sky-hook controller has been seen to perform poorly, the analytical minima is closer to the actual minima than the sky-hook solution.

By differentiating Eq. (16) with respect to t_0 and equating the zero, the following expression for the optimal centre of damping peak, t_{0opt}, as a function of damping width, $\bar{t}$, is obtained:

$$t_{0opt} = -\frac{1}{2}\tan^{-1}\left(\frac{\frac{\omega_n^2-\Omega^2}{4\Omega^2}+\left(\frac{\zeta_h-\zeta_l}{\pi}\right)^2(\bar{t}^2-\sin^2\bar{t})+\zeta_l\left(2\frac{\zeta_h-\zeta_l}{\pi}\bar{t}+\zeta_l\right)}{\frac{\Omega}{2\omega_n}\left(\frac{\zeta_h-\zeta_l}{\pi}\bar{t}+\zeta_l\right)}\right). \tag{17}$$

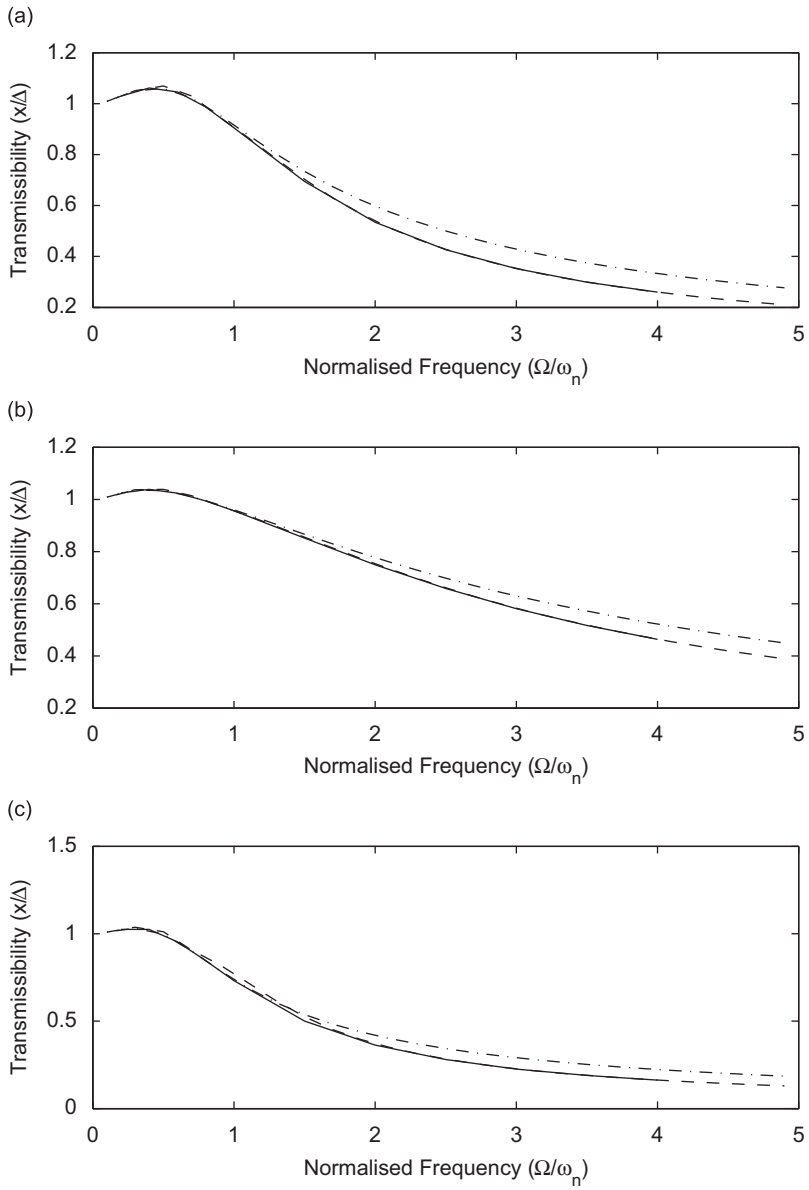

Fig. 10. Transmissibility plots comparing sky-hook, optimal and analytical switching times for (a) $\zeta_h = 1.5$ and $\zeta_l = 0.5$; (b) $\zeta_h = 2$ and $\zeta_l = 1$; (c) $\zeta_h = 2$ and $\zeta_l = 0.3$: – · – · – sky-hook, – – – analytical switching times, — optimal switching times.

By substituting Eq. (17) in Eq. (16), an algebraic function for $\overline{x}$ is obtained which is a function of a single control design parameter, $\overline{t}$. It is not possible to obtain an explicit analytical solution for the $\overline{t}$ value that minimising this function, however, an optimal $\overline{t}$ value can be obtained by numerically minimising the function with regard to $\overline{t}$ between the lower and upper bounds of 0 and π, respectively.

Plots comparing the transmissibility produced by the optimal and sky-hook switching times over a range of frequencies and damping values are shown in Fig. 10. These transmissibility plots show the performance of the sky-hook controller to be very close to that of the optimal controller below the undamped natural frequency. As frequency increases, the performance of the sky-hook controller diverges from the optimal.

In addition the analytical optimal solution based on Eq. (16) is shown (dashed line). It can be seen that this agrees excellently with the numerical optimal solution at frequencies above the natural frequency with a slight divergence at frequencies below the natural frequency. Note that the numerical optimal solution is plotted over a smaller frequency range in order for the analytical optimal solution to be more clearly visible.

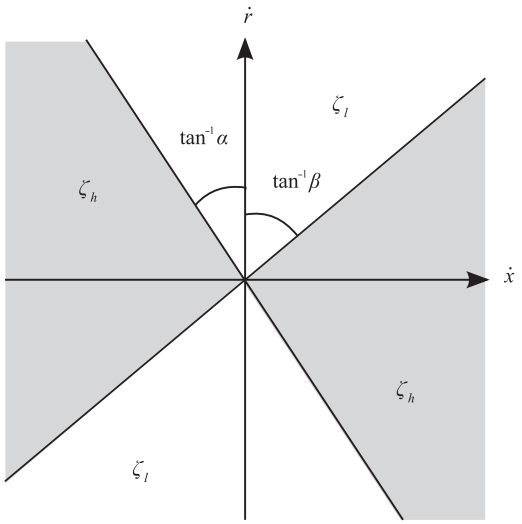

Fig. 11. Illustration of semi-active switching surfaces for generalised switching surface controller.

4. Switching surface control

The selection of parameters for the switching time controller discussed in the previous section requires knowledge of the frequency and phase of excitation. The appeal of the sky-hook form of control law is its simple form, use of readily measurable states and no requirement for explicit knowledge of the excitation. We seek to obtain a semi-active switching controller that is closer to optimal than sky-hook yet retains the practical characteristics of the sky-hook control form.

As discussed in Section 2 and illustrated in Fig. 3, the sky-hook control law may be thought of as a pair of switching surfaces. Considering the sky-hook controller in this manner naturally presents the question as to whether better isolation can be achieved by altering these switching surfaces.

For a switching surface to provide the same transmissibility for a given frequency regardless of amplitude it must be linear. A generalised form of semi-active switching surface control is expressed in Eq. (18), where α and β are the gradients of the linear surfaces. This controller is illustrated with-in the velocity plane in Fig. 11. The sky-hook controller is a specific case of this generalised form where $\beta=1$ and $\alpha=0$:

$$\zeta=\begin{cases}\zeta_h, & (\dot{x}+\alpha\dot{r})(\dot{x}-\beta\dot{r})>0,\\ \zeta_l, & \text{else.}\end{cases} \tag{18}$$

For $\beta=1$, the switching surface controller described by Eq. (18) is equivalent to that proposed by Verros et al. [20], in which the gradient of the second switching surface is designed to emulate the behaviour of specific sky-hook damping coefficients.

The numerical optimisation analysis in Section 3 may be extended to examine the nature of optimal switching surfaces. The steady-state velocities of the optimal switching time controlled system are shown in Fig. 12 for a number of excitation frequencies. The trajectories move outward from the centre with increasing frequency. The states at the high to low switching times are denoted by circles and the states at the low to high switching times are denoted by crosses. By plotting at multiple frequencies, these optimal switching states form optimal switching surfaces within the velocity plane.

These plots reveal that the optimal high to low switching surface is insensitive to damping values and is very close to the sky-hook switching surface of $\dot{x}-\dot{r}=0$, corresponding to a β value of 1. The optimal low to high switching surface, however, differs significantly from the sky-hook surface. The optimal surface is nonlinear and appears strongly dependant on the damping values. Below the natural frequency, the optimal switching surface is close to the sky-hook surface of $\dot{x}=0$, as is consistent with results from the switching times analysis. As frequency increases, the gradient of the surface diverges from that of the sky-hook surface.

As this optimal switching surface is nonlinear, it is not possible to define a low to high switching control surface that is optimal regardless of amplitude. However, as is illustrated in Fig. 13, over limited ranges of frequencies, the optimal surface may be approximated as linear.

Fig. 14 shows transmissibility plots of the switching surface controller expressed in Eq. (18), for $\beta=1$ and varying values of α. These plots show that it is possible to achieve isolation very close to optimal using a linear switching surface controller. From the low transmissibility obtained using a range of α values, it appears that amplitude trajectory is quite insensitive to switching state close to the optimal surfaces. This aids the process of control parameter selection by

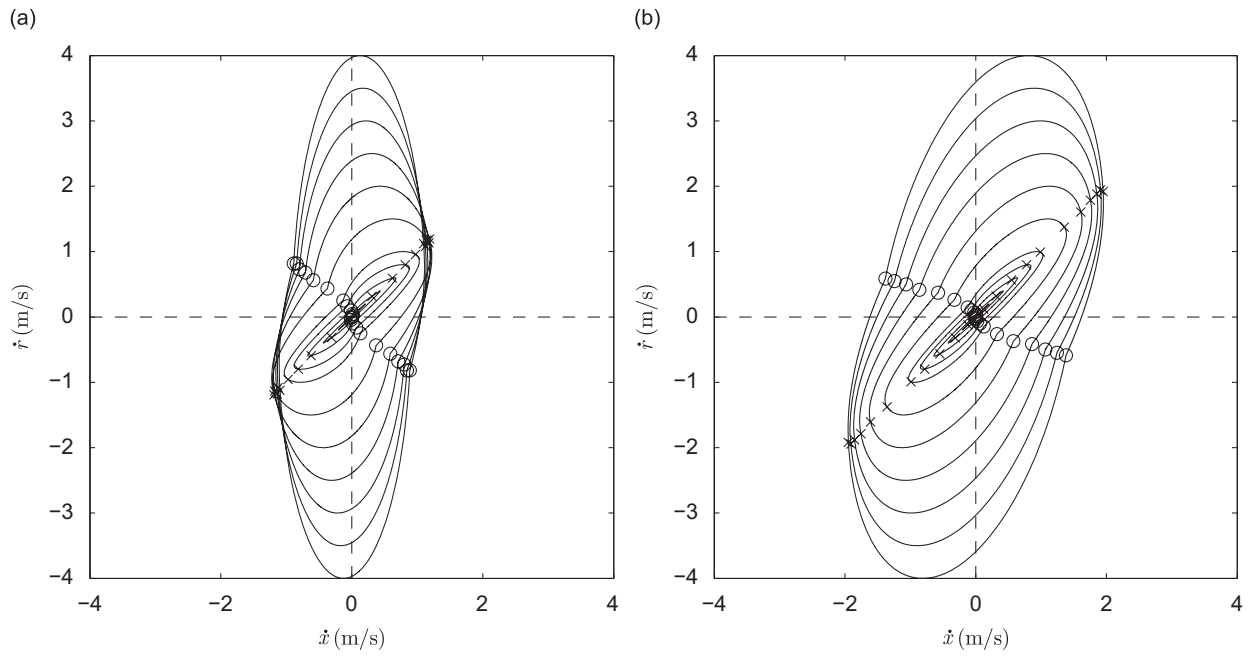

Fig. 12. Steady state velocities and switching states of optimal switching time controller over the frequency range $\Omega/\omega_n = 0.1-4$ for (a) $\zeta_h = 1.5$, $\zeta_l = 0.5$; (b) $\zeta_h = 2$, $\zeta_l = 1$: ○ high to low switching, × low to high switching.

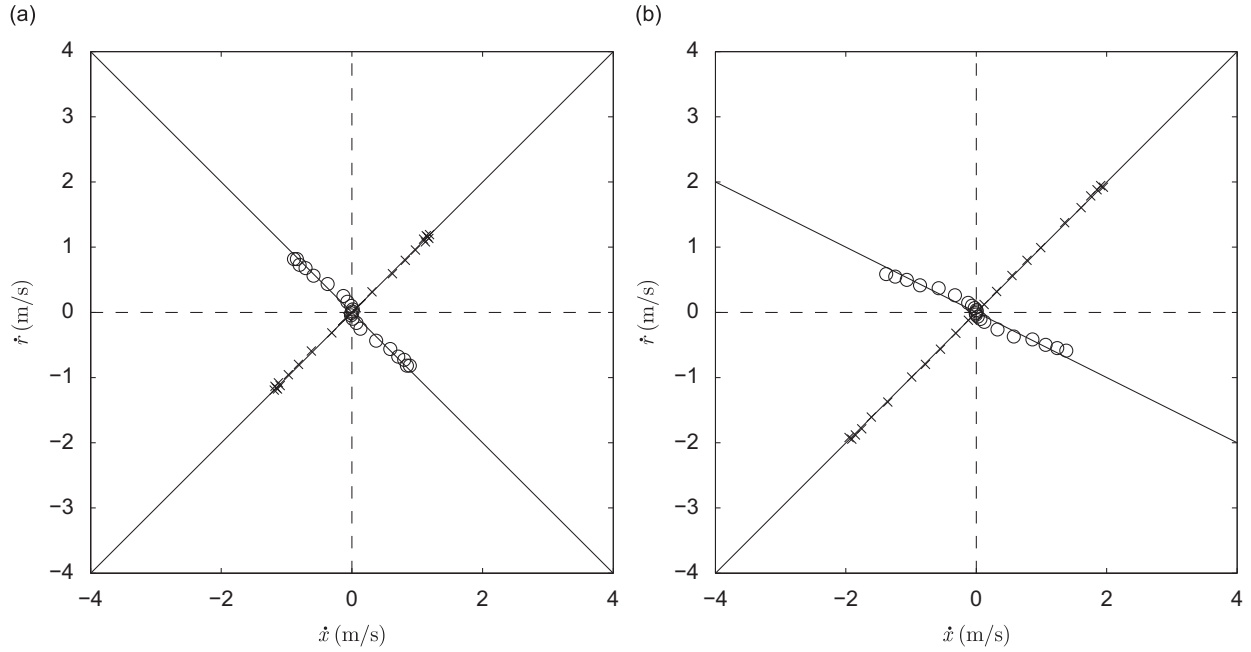

Fig. 13. Steady state switching states of optimal switching time controller and linear switching surface approximations over the frequency range $\Omega/\omega_n = 0.1-4$ for (a) $\zeta_h = 1.5$, $\zeta_l = 0.5$, $\alpha = 1$, $\beta = 1$; (b) $\zeta_h = 2$, $\zeta_l = 1$, $\alpha = 2$, $\beta = 1$: ○ high to low switching, × low to high switching.

providing relatively large tolerances. Over the range of damping values examined, an α value of 1 consistently produced isolation close to optimal, representing an improvement over the sky-hook controller (in which $\alpha = 0$) especially at frequencies above the natural frequency. It is therefore suggested that this value is an appropriate starting point for parameter selection.

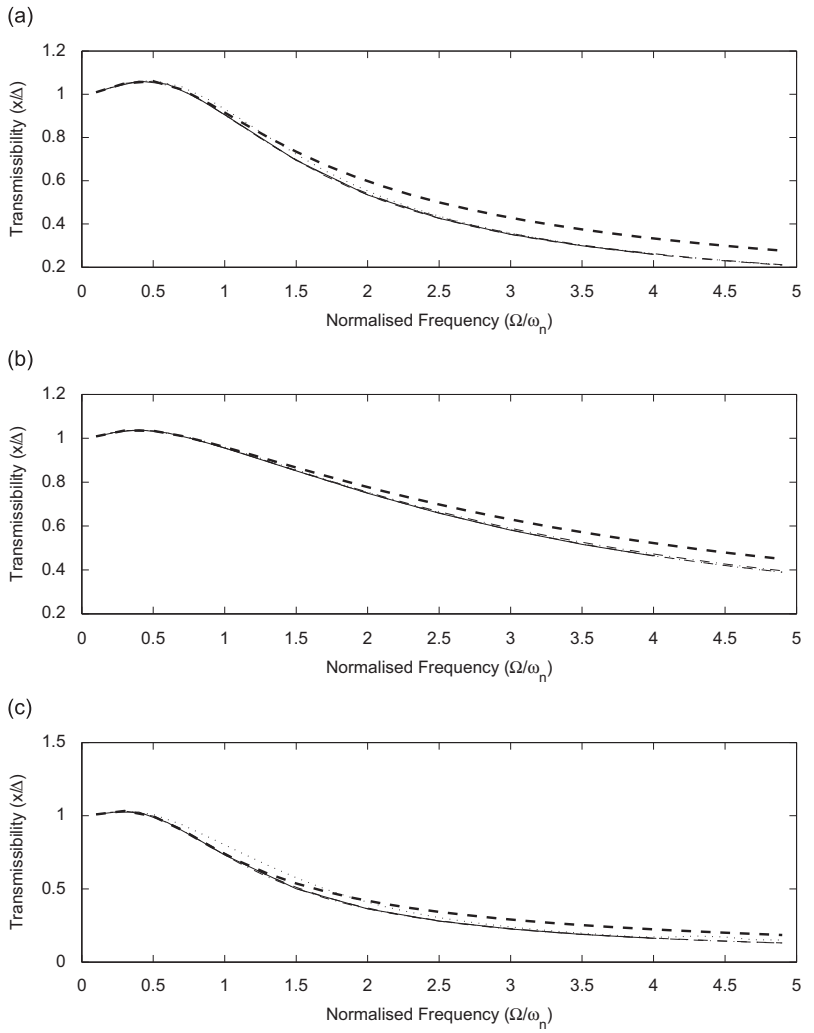

Fig. 14. Transmissibility plots of generalised switching surface controller and optimal solution for (a) $\zeta_h = 1.5$ and $\zeta_l = 0.5$; (b) $\zeta_h = 2$ and $\zeta_l = 1$; (c) $\zeta_h = 2$ and $\zeta_l = 0.3$: – – – – $\alpha = 0$ (sky-hook), – · – · – $\alpha = 0.5$, – – – $\alpha = 1$, ····· $\alpha = 10$, — optimal.

5. Conclusions

This paper has examined the form and behaviour of a sky-hook, semi-active control law when applied to a single degree of freedom, base isolating suspension system.

When the system is harmonically excited, in the steady-state, the sky-hook controller switches damping levels at two distinct times every half period of excitation.

By proposing and analysing a generalised switching controller with arbitrarily defined switching times, the optimality of the sky-hook switching conditions, with regard to minimising displacement transmissibility, is assessed. It is found that below the undamped natural frequency of the system, the sky-hook controller is close to optimal but diverges from the optimal switching times with increasing frequency.

An analytical solution is presented for the optimal switching times, based on a harmonic balance of the switching controller. For higher frequencies, where sky-hook control has been shown to be sub-optimal, the analytically approximated switching times are very close to optimal.

The sky-hook controller is then considered as consisting of two switching surfaces. Plotting the system states at the optimal switching times for multiple frequencies produces optimal switching surfaces. This reveals one of the sky-hook surfaces to be very close to optimal. The other optimal switching surface is shown to be nonlinear and dependent on damping values. A generalised form of linear switching surface control is presented. It is shown that, through appropriate parameter selection (a recommended guideline being $\alpha = 1$), this controller form, which retains the desirable practical attributes of sky-hook control, can achieve performance very close to optimal.

Acknowledgements

The authors would like to acknowledge the support of the EPSRC. Jack Potter is supported by an EPSRC DTA.

References

[1] B.F. Spencer Jr., S.J. Dyke, M.K. Sain, J.D. Carlson, Phenomenological model for magnetorheological dampers, *Journal of Engineering Mechanics* 123 (3) (1997) 230–238.
[2] S.-B. Choi, M.-H. Nam, B.-K. Lee, Vibration control of a MR seat damper for commercial vehicles, *Journal of Intelligent Material Systems and Structures* 11 (12) (2000) 936–944.
[3] C.-Y. Lai, W.H. Liao, Vibration control of a suspension system via a magnetorheological fluid damper, *Journal of Vibration and Control* 8 (4) (2002) 527–547.
[4] Y. Liu, T.P. Waters, M.J. Brennan, A comparison of semi-active damping control strategies for vibration isolation of harmonic disturbances, *Journal of Sound and Vibration* 280 (1–2) (2005) 21–39.
[5] M. Ahmadian, C.A. Pare, A quarter-car experimental analysis of alternative semiactive control methods, *Journal of Intelligent Material Systems and Structures* 11 (8) (2000) 604–612.
[6] R.S. Prabakar, C. Sujatha, S. Narayanan, Optimal semi-active preview control response of a half car vehicle model with magnetorheological damper, *Journal of Sound and Vibration* 326 (3–5) (2009) 400–420.
[7] J.-H. Kim, C.-W. Lee, Semi-active damping control of suspension systems for specified operational response mode, *Journal of Sound and Vibration* 260 (2) (2003) 307–328.
[8] M.J. Crosby, D.C. Karnopp, R. Harwood, Vibration control using a semi-active force generator, *Transactions of the ASME, Journal of Engineering for Industry* 96 (2) (1974) 619–626.
[9] Y. Shen, M.F. Golnaraghi, G.R. Heppler, Semi-active vibration control schemes for suspension systems using magnetorheological dampers, *Journal of Vibration and Control* 12 (1) (2006) 3–24.
[10] G.Z. Yao, F.F. Yap, G. Chen, W.H. Li, S.H. Yeo, Mr damper and its application for semi-active control of vehicle suspension system, *Mechatronics* 12 (7) (2002) 963–973.
[11] L.V.V. Gopala Rao, S. Narayanan, Sky-hook control of nonlinear quarter car model traversing rough road matching performance of lqr control, *Journal of Sound and Vibration* 323 (3–5) (2009) 515–529.
[12] L.M. Jansen, S.J. Dyke, Semiactive control strategies for mr dampers: comparative study, *Journal of Engineering Mechanics* 126 (8) (2000) 795–803.
[13] H. Li, M. Liu, J. Li, X. Guan, J. Ou, Vibration control of stay cables of the shandong binzhou yellow river highway bridge using magnetorheological fluid dampers, *Journal of Bridge Engineering* 12 (4) (2007) 401–409.
[14] E.A. Johnson, G.A. Baker Jr., B.F. Spencer, Y. Fujino, Semiactive damping of stay cables, *Journal of Engineering Mechanics* 133 (1) (2007) 1–11.
[15] Y.F. Duan, Y.Q. Ni, J.M. Ko, Cable vibration control using magnetorheological dampers, *Journal of Intelligent Material Systems and Structures* 17 (4) (2006) 321–325.
[16] S.J. Dyke, B.F. Spencer Jr., M.K. Sain, J.D. Carlson, An experimental study of mr dampers for seismic protection, *Smart Materials and Structures* 7 (5) (1998) 693–703.
[17] B. Erkus, M. Abé, Y. Fujino, Investigation of semi-active control for seismic protection of elevated highway bridges, *Engineering Structures* 24 (3) (2002) 281–293.
[18] Q. Zhou, S.R.K. Nielsen, W.L. Qu, Semi-active control of shallow cables with magnetorheological dampers under harmonic axial support motion, *Journal of Sound and Vibration* 311 (3–5) (2008) 683–706.
[19] F. Verhulst, *Nonlinear Differential Equations and Dynamical Systems*, Springer, New York, Inc., 1990.
[20] G. Verros, S. Natsiavas, G. Stepan, Control and dynamics of quarter-car models with dual-rate damping, *Journal of Vibration and Control* 6 (7) (2000) 1045–1063.